Natural diatomites: Efficient green catalyst for Fenton-like oxidation of Orange II

N. Inchaurrondo [a,*], J. Font [b], C.P. Ramos [c], P. Haure [a]

[a] Departamento de Ingeniería Química, Div. Catalizadores y Superficies—INTEMA—CONICET, Universidad Nacional de Mar del Plata, Mar del Plata 7600, Argentina
[b] Departament d'Enginyeria Química, Escola Tècnica Superior d'Enginyeria Química, Universitat Rovira i Virgili, Tarragona, 43007 Catalonia, Spain
[c] Departamento de Física de la Materia Condensada, GiyA-CAC-CNEA, Av. Gral. Paz 1499 San Martín, Buenos Aires, Argentina

ABSTRACT

The Fenton-like oxidation of the anionic azo-dye Orange II (100–500 mg/L) was batchwise performed using commercial grade diatomites (3.5% Fe content) thermally treated.

Solid samples were thoroughly characterized by several techniques. Peroxidation experiments were performed varying the diatomite calcination temperature (500, 700, 1000 °C), reaction temperature (50, 60, 70, 80 °C), catalyst load (0.47, 0.94, 1.89 and 3.78 g), H_2O_2 concentration (11.0, 13.7, 20.6 mmol/L) and dosing, pH (2–3.5) and initial dye concentration (0.28, 0.57, 1.43 mmol/L). The influence of NaCl and oxalic acid on the catalytic performance and stability was also addressed.

The best results were obtained with samples calcined at 700 °C, with initial pH 3, at 70 °C and using the stoichiometric amount of H_2O_2, since complete decoloration, TOC reduction close to 67% and negligible Fe leaching were achieved. The stability of the catalyst maintains after 20 h of usage, with a final Fe loss of 2.25%. An average of 0.88 mg/L of iron leached after each run, which is below the discharge limit.

© 2015 Elsevier B.V. All rights reserved.

1. Introduction

Diatomite occurs as abundant sedimentary accumulations of siliceous skeletons (frustules) of microscopic aquatic plants known as diatoms [1]. Its composition mainly includes opal or hydrous silica (SiO_2–H_2O), usually 70–90%, but also alumina (0.6–8%), iron (0.2–3.5%), alkali metal oxides, Na_2O and MgO (less than 1%), CaO (0.3–3%) and minor amounts of other impurities, such as P_2O_5 and TiO_2 [2]. Sand, clay, carbonate and organic material are typical contaminants, however the latter ones decompose into gaseous CO_2, SO_2 and H_2O during calcination, leaving the bulk of diatomite [3]. Due to its extremely porous structure, low density and high surface area, they are used for adsorption of organic chemicals [2,4–8] and heavy metal removal [9–13].

Diatomite has also been employed as a catalyst support for several reactions: oil hydrogenation [14], hydration of acrylonitrile [15], Fischer–Tropsch synthesis [16], hydrocarbons oxidation [1], photodegradation of industrial wastes [17,18], photoelectro-

Fenton of industrial wastewaters [19], and phenol hydroxylation [20]. Nevertheless, the use of diatomite as a catalyst rather as catalyst support has not been extensively studied [21], although, the presence of a high percentage of iron would enable its use as a heterogeneous Fenton-like catalyst without requiring major modifications.
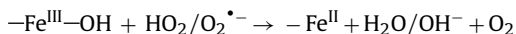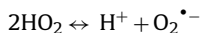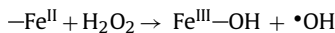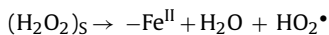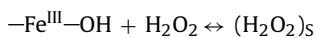
The closest antecedent to the employ of this material in Fenton processes is the use of zeolites, clays and natural oxides. These materials have been widely tested in Fenton-like oxidation reactions, giving in several cases a high level of mineralization and reduced leaching of the active phase [22–24]. Also, the study of pillared clays (PILC) as Fenton catalysts has been frequently reported, being the preferred materials for the degradation of organic pollutants [24].

There is not a full consensus about the Fenton-like mechanism with supported iron species and this is related to the variation in the Fe coordination environment in diverse materials, such as pure iron oxides, clays or diatomites.

* Corresponding author. Fax: +54 2234810046.
E-mail address: ninchaurrondo@gmail.com (N. Inchaurrondo).

Lin and Gurol [25] studied the decomposition of H_2O_2 on iron oxide and summarized the mechanism of Fe^{3+}-initiated chain reaction through the following sequence:

$$-Fe^{III}-OH + H_2O_2 \leftrightarrow (H_2O_2)_S$$

$$(H_2O_2)_S \rightarrow -Fe^{II} + H_2O + HO_2^{\bullet}$$

$$-Fe^{II} + H_2O_2 \rightarrow Fe^{III}-OH + {}^{\bullet}OH$$

$$2HO_2 \leftrightarrow H^+ + O_2^{\bullet-}$$

$$-Fe^{III}-OH + HO_2/O_2^{\bullet-} \rightarrow -Fe^{II} + H_2O/OH^- + O_2$$

The initiation reaction in systems involving iron oxides is expected to be the interaction of H_2O_2 with Fe(III) sites on the surface. The reactions are initiated by the formation of a precursor surface complex of H_2O_2 with the oxide surface. The protonation equilibria of unoccupied surface groups, that is, the species $-Fe^{III}-OH_2^+$ and $-Fe^{III}-O^-$, affects the H_2O_2 decomposition. Furthermore, under acidic conditions the dissolution of iron oxides occurs and the presence of some organic compounds generates the iron solubility via complexation and reductive dissolution, which promotes the homogeneous Fenton contribution [26].

The different activity of iron supported catalysts is influenced by the cation dispersion in the support, iron valence, surface area, point of zero charge, and the presence of different iron species, for example in clays, iron could be in the form of free iron oxides, structural iron in the clay lattice or complexed iron [27].

The application of diatomite as a Fenton catalyst is attractive and innovative as it is a low cost material, widely available from a sustainable source with a high content of Fe, key in the Fenton reaction mechanism. These characteristics agree well with some of the "green chemistry" principles, such as the employment of alternative feedstocks that are more innocuous and the design of eco-compatible chemicals [28]. In this context, the aim of this study is to explore the use of natural Argentinian diatomite as a Fenton-like catalyst for the degradation of Orange II (OII), which belongs to the wide family of the azo-dyes.

Orange II, also known as Acid Orange 7, has a synthetic origin and a complex aromatic structure with two aromatic rings (a benzene ring and a naphthalene ring), a sulfonated group and an azo bond ($-N=N-$). This poorly biodegradable azo-dye is widely used in the dyeing of textiles and cosmetics, and extensively found in the wastewaters of the related industries [29]. For this reason, several authors have investigated the OII degradation through Fenton and Fenton-like processes as listed in Table 1.

Most researchers obtained high OII conversions, but rarely report TOC reduction data. Using heterogeneous catalysts, best results in terms of decoloration and TOC reduction (only owned to peroxidation) were obtained by Ramírez et al. [30,31] for the oxidation of 35 mg/L solutions of OII using high loaded Fe-saponite based samples. With higher OII concentrations (100 mg/L), best results were obtained with the homogeneous reaction [32].

According to the literature, there exists a complex network of interactions between the species involved in the Fenton process, which depends on the concentration of oxidant, catalyst and pollutant, catalyst nature, pH and temperature. All of these parameters define the efficiency of the process and the degree of mineralization. Therefore, in the present study, several operating conditions were studied to evaluate the performance of commercial diatomites thermally treated for their use as a Fenton-like catalyst over the oxidation of Orange II.

2. Experimental

2.1. Catalyst preparation

The diatomite sample was purchased from a local supplier (Marysol), harvested from a deposit located in Ing. Jacobacci, Río Negro, Argentina. The raw diatomite was sieved and the fraction 7–8 mesh (2.38–2.83 mm) collected. Then, it was separated in different portions, which were subsequently calcined at three different final temperatures, 500, 700 and 1000 °C, under air atmosphere in a programmable furnace, applying a heating rate of 10 °C/min, from room temperature to the selected calcination temperature. The samples were left in the furnace for 5 h at the calcination temperature.

2.2. Catalyst characterization

The Fe content of the catalyst was determined by inductively coupled plasma-atomic emission spectroscopy (ICP-OES, Spectro Arcos) after microwave-assisted digestion of the samples.

Specific surface area and pore volume of the catalysts were determined by N_2 adsorption/desorption at 77 K, using a Micromeritics ASAP 2000 surface analyzer. The samples were outgassed overnight at 523 K prior to the adsorption analysis.

Powder X-ray diffraction (XRD) patterns of the samples were obtained with a Siemens model of D5000 diffractometer employing Cu Kα radiation. The X-ray was operated at 40 kV and 30 mA. The patterns were recorded over $5° < 2\theta < 75°$ angles, and compared to the X-ray powder files to confirm phase identities.

Thermogravimetric analyses (TGA) were performed in a TGA-50 Shimadzu equipment with thermal analyzer TA-50 WSI, using a heating rate of 10 °C/min, under an oxygen flow of 30 mL/min. Diatomites were pulverized and samples of 20 mg were taken. The curves were recorded simultaneously along with the temperature increment.

The chemical composition analysis of samples was performed by X-ray fluorescence (XRF) using a Philips PW2540 Magix spectrophotometer yielding the weight percentage of each constituting element. A constraint of X-ray fluorescence spectroscopy is its inability to analyze elements with an atomic number below 11 (Na).

The surface morphology was investigated by means of a scanning electron microscope JEOL JSM-6460LV. The elemental composition was determined by energy dispersive X-ray spectroscopy (EDS) using an EDAX Genesis XM4-Sys60 equipment.

Different species in the sample were identified by Fourier transform infrared/attenuated total reflection spectroscopy, (FTIR/ATR Nicolet 6700). Spectra were recorded in the region of $4000–400\ cm^{-1}$, at room temperature by performing 64 scans with a resolution of $2\ cm^{-1}$.

Mössbauer spectra were obtained at room temperature (RT) with a conventional constant acceleration spectrometer in transmission geometry with a ^{57}Co/Rh source. Measurements were recorded at 10 mm/s and then fitted using the Normos program developed by Brand [44]. Isomer shift values are given relative to that of α-Fe at RT.

The point of zero charge (PZC), where the total concentration of surface anionic sites equals the total concentration of surface cationic sites, was determined by the mass titration method, reported by Preocanin and Kallay [45]. Finally, the surface charge was determined by the acid titration method [46].

Table 1
Oxidation of Orange II in heterogeneous and homogeneous Fenton processes at soft pressure and temperature.

Catalyst	OII conversion (%)	TOC conversion (%)	pH	Operating conditions	Leaching	Ref.
Fe-saponite	96 (30 °C), 99 (70 °C)	82 (30 °C), 91 (70 °C)	3	OII 35 mg/L, H_2O_2 6 mmol/L, cat. 90 mg/L (17% Fe), 30, 70 °C, 4 h.	<1 mg/L	[30]
Pillared clay Fe-saponite	100	> 85	3	OII 35 mg/L, H_2O_2 13.8–24.8 mmol/L, cat. 60–120 mg/L (26.2% Fe), 40–70 °C, 3 h.	<3%	[31]
Fe^{2+}	100	70	3	OII 105 mg/L, H_2O_2 13.8 mmol/L (1.1 stoich.), Fe:H_2O_2 = 0.05% wt (23.5 mg/L of Fe), 50 °C, 2 h.	Homogeneous reaction	[32]
Carbon-Fe (M-Fe)	100	80 (30 °C), 83 (50 °C), 87 (70 °C) Around 50% of adsorption at 30 °C	3	OII 35 mg/L, H_2O_2 101 mg/L (0.71 of stoich.), 0.2 g/L cat. (0.7% Fe), 30, 50, 70 °C, 4 h.	0.97 (30 °C), 1.35 (50 °C) and 1.6 (70 °C) mg/L	[33]
M-Fe (carbon aerogels)	100	Not reported	3	OII 35 mg/L, H_2O_2 6 mmol/L, cat. 0.2 g/L (3.5% Fe), 30 °C, 3 h.	1–2%	[34]
Magnetite vanadium–titanium	100	30	3	OII 70 mg/L, H_2O_2 10 mmol/L, cat. 1 g/L, 20 °C, 4 h.	Not reported	[35]
Fe-EDTA	90	Not reported	7	OII 70 mg/L, H_2O_2 10 mmol/L, cat. 2 mmol/L, 20 °C, 10 min.	Homogeneous reaction	[36]
Fe^{2+}	>95	Not reported	3	OII 50 mg/L, H_2O_2 2.94 mmol/L, cat. 15 mg/L, 20 °C, 30 min.	Homogeneous reaction	[37]
Carbon-Fe (N-Fe)	100	60	3	OII 35 mg/L, H_2O_2 6 mmol/L, cat. 0.1 g/L (7%), 30 °C, 4 h.	<1.7%	[38]
$FeVO_4$	93	Not reported	6	OII 100 mg/L, H_2O_2 15 mmol/L, cat. 0.5 mg/L, 30 °C, 1 h.	Fe < 1 mg/L V < 3 mg/L	[39]
Fe	100	39	3	OII 105 mg/L, H_2O_2 200 mg/L, cat. 20 mg/L, 30 °C, 1 h.	Not reported	[40]
Fe^{III}- TAML	61	35	10	OII 35 mg/L, H_2O_2 10 mmol/L, cat. 0.0002 mmol/L, 25 °C, 30 min.	Not reported	[41]
Montmorillonite	90	Not reported	3	OII 20 mg/L, H_2O_2 4 mmol/L, cat. 0.,2 g/L (4.8% Fe), 30 °C, 40 min.	8%	[42]
Mn (II)	100	Not reported	8.5	OII 17.5 mg/L, H_2O_2 10 mmol/L, cat. 0.02 mmol/L, 25 °C, 40 min.	Homogeneous reaction	[43]

2.3. Oxidation tests

In a typical experiment, a specific amount of diatomites was added into 170 mL of 0.1 g/L (0.28 mmol/L) of OII (Biopack, 95%) in a 250 mL thermostated batch reactor equipped with a refrigerant. To minimize external mass transport effect, experiments were performed with vigorous agitation. In all cases, the initial pH was fixed by the addition of H_2SO_4 (2 mol/L). During the reaction, pH was monitored but not controlled. In such conditions, the mineralization reaction is stated to be [47,48]:

$$C_{16}H_{11}N_2NaO_4S + 42H_2O_2 \rightarrow 16CO_2 + 46H_2O + 2HNO_3 + NaHSO_4$$

Once the reaction temperature was reached, a given volume of 30% wt. hydrogen peroxide (Cicarelli) was added into the system and the reaction started. Most of the experiments were performed with the stoichiometric demand of H_2O_2 (13.7 mmol/L) for the complete mineralization of OII (0.28 mmol/L).

Samples were withdrawn at different time intervals and promptly analyzed to determine pH, and OII, hydrogen peroxide and total organic carbon (TOC) concentrations. In order to select the most appropriate reaction conditions, experiments were performed varying temperature, initial pH and catalyst, OII and H_2O_2 concentrations.

The efficiencies of hydrogen peroxide consumption described by Zazo et al. [49] as the ratio between TOC consumed and hydrogen peroxide decomposed at a given reaction time (η) and the amount of TOC consumed per unit weight of hydrogen peroxide fed (ϵ) were defined as:

$$\eta = \frac{\text{TOC consumpsion (mg)}}{H_2O_2 \text{ consumption (g)}} \quad (1)$$

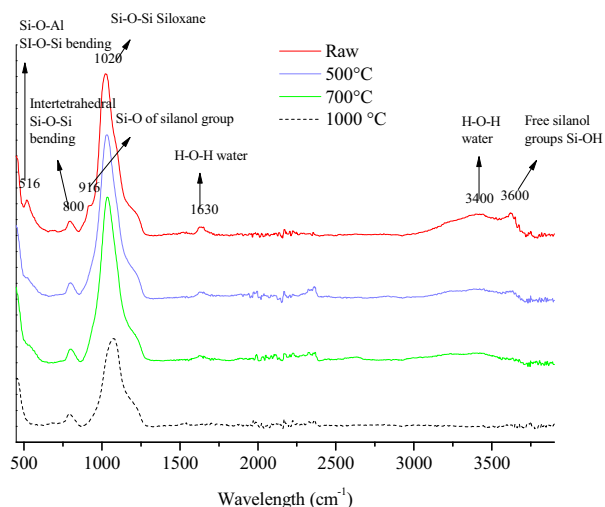$$\epsilon = \frac{\text{TOC consumpsion (mg)}}{H_2O_2 \text{ fed (g)}} \quad (2)$$

Fig. 1. FTIR spectra of the raw diatomite and samples calcined at different temperatures (500, 700, 1000 °C).

2.4. Analyses

The OII solution decoloration was evaluated at 485 nm using a SHIMADZU UV-1800 spectrophotometer (sample of 1 mL diluted 1:3). Hydrogen peroxide concentration was determined by a Glycemia enzymatic test (Wiener Lab) with a sample of 20 μL. Total organic carbon (TOC) was determined in a TOC analyzer (Shimadzu, model TOC-VCPN). pH was determined using a Black Stone pH controller. Total Fe concentration leached in the supernatant was measured using a commercial kit (FeVer 2™, Hach). Reported values are the average of at least two measurements, and error bars represent the standard deviation.

3. Results and discussion

3.1. Catalyst characterization

The raw and calcined samples were characterized together with a sample used in OII oxidation tests (0.94 g of diatomite calcined at 700 °C, 0.28 mmol/L of OII, 13.7 mmol/L of H_2O_2, initial pH 3, 70 °C). The catalyst was used in five consecutive oxidation reactions of four hours each, without treatment of the diatomite sample between tests.

3.1.1. FTIR

Fig. 1 depicts the main absorption bands for raw diatomite, found at 3600, 3400, 1630, 1020, 916, 800 and 516 cm^{-1}. The band at 3600 is due to the free silanol group (SiO—H stretching) but could also be attributed to the O—H vibration mode of hydroxyl groups of kaolinite [2,11]. The broad band centered at 3400 cm^{-1} is attributed to the O-H stretching of physically adsorbed water and the band at 1630 represents the H—O—H bending vibration of water [2,11,50]. The signal at 1020 cm^{-1} corresponds to the siloxane (—Si—O—Si—) group stretching and the 916 cm^{-1} band corresponds to the stretching of the silanol group (Si—OH) and/or to the Al–Al—OH bending (clay impurity). The 800 cm^{-1} band is related to the free silica and/or quartz and is found in all starting diatomite materials (intertetrahedral Si—O—Si bending). The peak at 516 cm^{-1} is attributed to the Si—O—Si and/or Si—O—Al (related to the octahedral sheet) bending vibration [11].

The calcination produced the dehydroxylation of the diatomite samples (elimination of the OH stretching from Si—OH and Al–Al—OH bond at 916 cm). The peak corresponding to Si—OH, originally present on the surface of diatomite, remarkably decreased in
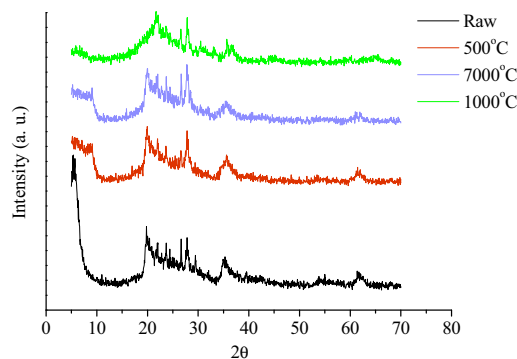

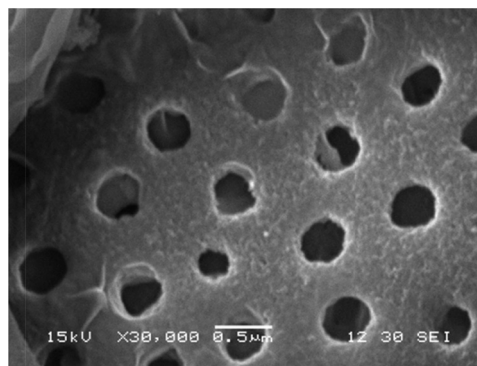**Fig. 2.** XRD spectra of raw diatomite and samples calcined at 500, 700 and 1000 °C.

Fig. 3. Pores in the diatom frustule.

intensity upon calcination (3600 cm^{-1}) [2] and this process led to the formation of surface siloxane groups or —Si—O—Si— bridges. The broad band at 3400 cm^{-1} and the peak at 1630 cm^{-1}, related to the presence of adsorbed water, gradually disappeared. The band at 1020 cm^{-1} was reduced after calcination and the peak found at 516 cm^{-1} disappeared. This suggests that the clay mineral structure was damaged with calcinations [11]. The band related to the free silica at 800 cm^{-1} was not affected by the thermal treatment.

No differences were detected between the FTIR spectra of the used and fresh sample (see Fig. SD1 in Supplementary material).

3.1.2. XRD

Fig. 2 shows the XRD spectra obtained from the raw and calcined diatomites. The amorphous silica phase (opaline silica) is characteristic of the frustules composition (broad reflection centered at 20–25°) [9]. The XRD patterns of diatomite samples show the presence of quartz (SiO_2) (27°) and albite (feldspar Na(AlSi$_3$O$_8$) 28°, 24°, 22°). The amorphous phases of natural diatomite are transformed into a crystalline structure, cristobalite (36°), at 1000 °C, as observed by other authors [50].

The XRD patterns did not show peaks related to iron oxides. However this technique is not sensitive enough if the phase amount is too low (less than 5 wt%). Moreover, if the particle size of iron oxide is very small, XRD patterns cannot detect them.

According to FRX and EDX results, a part of the diatomite may be composed by several clay minerals [2,3,50]. In effect, by XRD, a substantial content of nontronite is evident (main peak at 5–6°). The disappearance of those peaks upon calcinations may indicate the removal of the clay mineral. In addition, FRX pinpointed a calcium derivate that could be related to the presence of calcite (29°), a crystallized calcium carbonate phase.

The spectrum of the used sample does not differ from the spectrum of the fresh one. The reaction takes place at mild conditions;
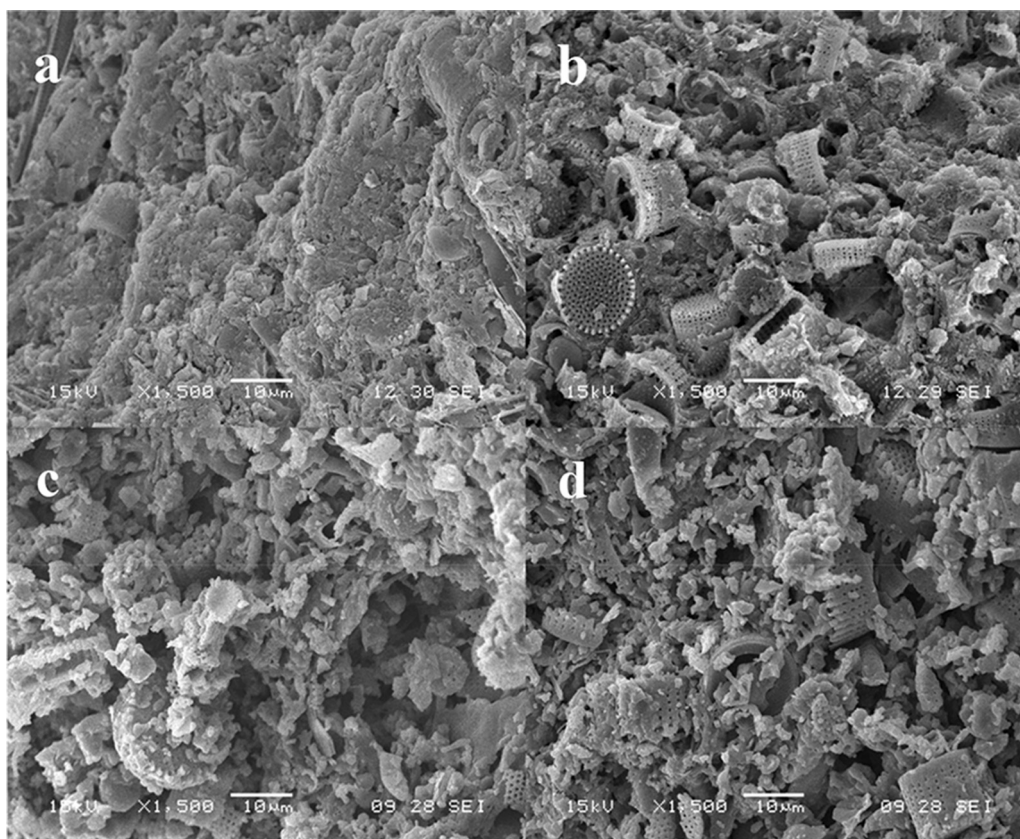
Fig. 4. SEM images (×1500) of raw diatomite (a) and samples calcined at different temperatures 500 (b), 700 (c) and 1000 °C (d).

therefore there is no modification of the catalyst phases (see Fig. SD2 in Supplementary material).

3.1.3. SEM/EDX

The SEM micrograph of the natural diatomite shows a dominant presence of *Aulacoseira alpigena* and, at less extent, *Fragilaria* (see Fig. SD3 a–f in Supplementary material). The diatom presents a nearly regular array of submicron pores (250–500 nm) as Fig. 3 illustrates.

SEM images (Fig. 4a–d) reveal that the thermal treatment at 500 °C eliminated some impurities on the surface, allowing a better visualization of frustules. Calcination at higher temperature caused the partial loss of the skeletal structure, but the original geometry was mostly preserved.

The mapping of Fe on the diatomite surface showed that the metal is homogeneously dispersed (see Fig. SD4 in the Supplementary material).

The weight composition of the raw and calcined samples obtained by EDX is given in Table 2. The composition of the different samples is approximately the same since the weight loss during calcination was very low. The chemical composition reveals the presence of oxides of Si and Al together with other mineral impurities, i.e. Fe, Na, Ca, Mg, etc.

The used sample presents no significant variation of the Fe content since the cation leaching through five oxidation reactions is negligible.

The color of the calcined materials changed from white to brown-red. This may be attributed to the migration of iron ions to the surface; as well as the conversion of different iron bearing minerals to Fe_2O_3 [51]. The Fe weight percentage was measured through EDX in different regions of the raw sample and the diatomite calcined at 1000 °C (see Fig. percentage of iron is higher near the surface due to the migration of ions during calcination [51].

No modification of the catalyst morphologic characteristics occurs after the OII oxidation reaction. The SEM images of the used sample do not differ from the images of the fresh catalyst (see Fig. SD6 in the Supplementary material).

Table 2
Composition by EDX of fresh and used samples.

	Wt (%)				
	Raw	500	700	1000	Used sample
C	18	9,5	9,1	10	12,7
O	39,2	46,5	41,3	40,6	39,6
Na	0,2	0,3	0,41	0,29	0,66
Mg	1,6	1,1	1,1	0,9	1,58
Al	4,7	6,6	7,2	5,5	6,7
Si	33	32,3	36,6	37,7	34,6
Ca	0,23	0,84	0,9	0,7	0,55
Fe	3	2,7	3,3	4,3	3,7

Table 3
Iron content (%).

Sample	% Fe
Raw	3.0
500 °C	3.5
700 °C	3.6
1000 °C	3.5

Table 5
BET surface area, pore volume and half pore with of fresh and used samples.

Sample	BET area (m²/g)	Pore volume (cm³/g)	Half pore width (nm)
Raw	121	0.29	4.1
500 °C	108	Not measured	Not measured
700 °C	76	0.26	3.7
1000 °C	5	0.015	7.0
Used sample	115	Not measured	Not measured

3.1.4. Fe content

The Fe content of the catalyst was determined by inductively coupled plasma-atomic emission spectroscopy (ICP-OES) after microwave-assisted digestion of samples. Results are presented in Table 3 with a 0.5 standard deviation value. Results are in agreement with the values obtained by EDX.

3.1.5. XRF

The XFR analysis (Table 4) showed that silica represents the major constituent of diatomite samples whereas mineral components (metal oxides) contribute to the rest of the composition, with a relative high concentration of iron. Data revealed that the thermal treatment does not modify the composition determined by XRF.

Carbon is not detected because this technique identifies atomic numbers larger than fluorine.

The XRF compositions of the fresh and used samples do not differ.

3.1.6. BET surface area and pore distribution

BET surface area, pore volume and half pore width of the diatomite samples are presented in Table 5.

The calcination generates the shrinkage and hardening of individual particles as well as the formation of agglomerates or clusters of particles through fusion (sintering). These processes may contribute to the reduction of the surface area, especially in the sample calcined at 1000 °C, where the sintering process may have been more extensive. Moreover, the removal of impurities might decrease the surface area, considering that the impurities micropores give larger surface area compared to the diatom skeleton [13]. This could explain the surface area drop in sample calcined at 700 °C, giving a practically unchanged pore volume and half pore width.

The catalyst used in successive tests showed an increment of the BET area probably related to the removal of impurities under an acidic media in the presence of an oxidant.

The pore distribution is presented in Fig. 5. The calcination at 700 °C caused the elimination of 1 nm micropores, and further calcination at 1000 °C reduced the pore volume giving importance to macropores (7 nm).
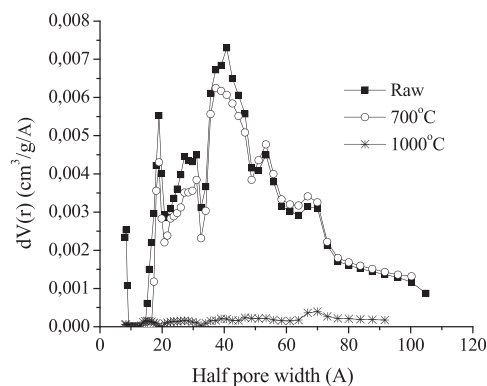
Fig. 5. Pore distribution of raw and calcined samples.

3.1.7. Thermogravimetric analysis

The first zone of weight loss (20–200 °C) is due to the removal of strongly adsorbed water, followed by the dehydroxylation of some associated silanol groups on the external surface of the diatomite [8], decomposition of organic matter (especially in the raw sample) and clay minerals [52,53]. Between 200 °C and 900 °C, raw diatomite and samples calcined at 500, 700 and 1000 °C undergo a weight loss of 4.21, 1.87, 1.03 and 0%, respectively. As a result, the Fe percentage slightly increases after the calcination of the raw diatomite, but it is assumed that the iron percentage in diatomites calcined at 1000 °C is basically the same than the value measured for the other samples (see Fig. SD7 in the Supplementary material).

3.1.8. Mossbauer spectroscopy

The room temperature Mössbauer spectra of the studied samples are shown in Fig. 6 and the corresponding hyperfine parameters are displayed in Table 6.

The raw material sample was fitted to two overlapping doublets reflecting that all the iron in the sample is as Fe^{3+}. The major doublet (D1) is typical of Fe^{3+} in *cis* octahedral (M2) sites of smectites and related minerals [54–58]. The octahedral Fe seems to be in an environment somewhat similar to that of nontronite (iron-rich end member of the smectite group), which is normally *trans* vacant [59,60]. The minor doublet (D2) is consistent with some tetrahedral Fe^{3+}.

For the samples calcined at 500 °C and 700 °C, an increase in QS in the octahedral sites is the product of a dehydroxylation of the octahedral planes of the clay. This process releases water from the tetrahedral sheets, so the number of ligands of the octahedral iron reduces in some of the octahedrons of the clay structure. The other octahedrons slightly distort and the iron site symmetry reduces. In particular for the sample calcined at 500 °C, a different Fe^{3+} doublet (D3) corresponding to dehydroxylated surface sites was necessary to a better fit of the spectrum.

In the sample calcined at 1000 °C, the iron site environment becomes more symmetric (due to changes in the electric field gradient at the Fe^{3+} nucleus maybe provoked by differences in O—Fe—O bond angles and lengths) and as a consequence, the QS decreases. An appreciable amount of Fe_2O_3 is also detected in this spectrum, represented by the magnetic sextet pattern (S). The hyperfine mag-
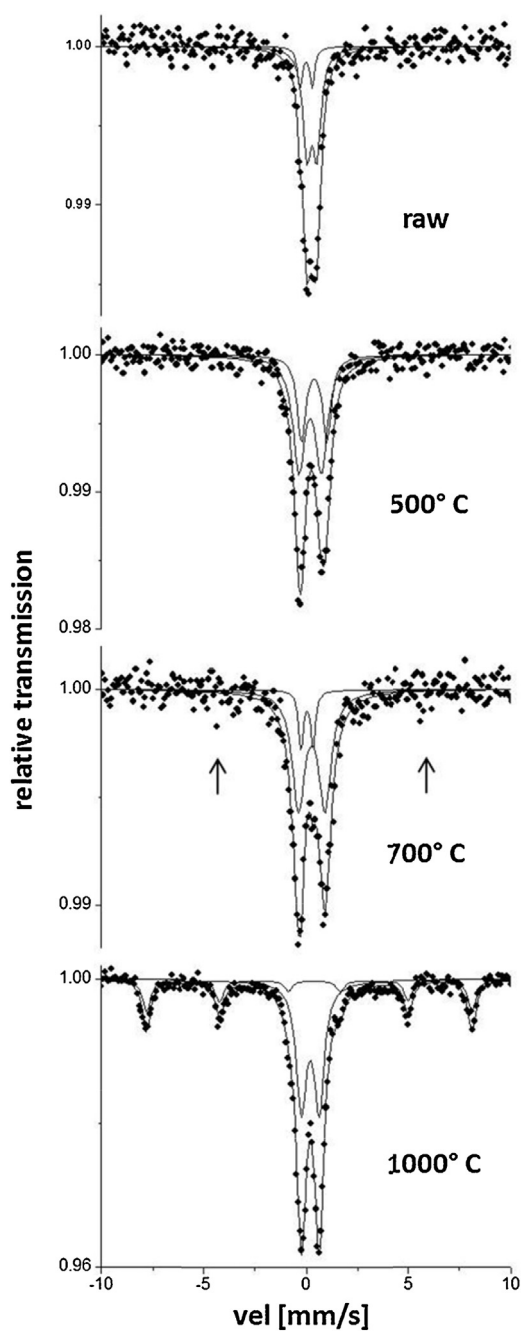
Table 4
Composition by XRF (wt/wt%) of fresh and used samples.

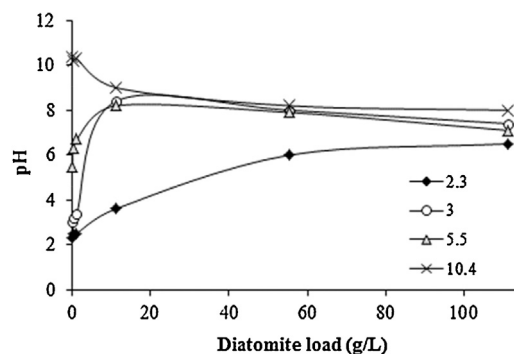| Sample	Al	Si	K	Ca	Ti	Fe
Raw	12.0	63.0	1.80	4.46	1.49	17.5
500 °C	12.0	62.9	1.40	4.86	1.48	17.4
700 °C	13.0	62.5	1.50	4.29	1.45	17.6
1000 °C	13.0	62.5	1.40	4.36	1.34	17.8
Used sample	12	63	1.4	4.88	1.5	17.4

Fig. 7. Mass titration with different initial pH (2.3; 3; 5.5; 10.4).

netic field value obtained is somewhat smaller than that reported in literature for pure well crystallized hematite (51.7 T). This could be due to an eventual Fe for Al substitution and/or to the influence of the particle size.

Even if in the case of the sample calcined at 700 °C the resolution of the spectrum is not enough to fit a magnetic contribution – which seems to be masked in the background – maybe a scarce content of Fe_2O_3 is also present in the sample (as can be seen in Fig. 6 arrows).

3.1.9. Point of zero charge (PZC)

The hydroxyl groups present on the surface of diatomite can gain or lose a proton, resulting in a surface charge that varies with pH. At pH < PZC, surface sites are protonated and the surface becomes positively charged; while at pH > PZC, the surface hydroxides lose their protons and the surface becomes anionic [61]:

$$H^+ + MOH \rightarrow MOH_2^+$$

$$MOH \rightarrow H^+ + MO^-$$
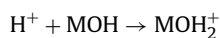
In silica supports the active exchange sites are the silanol groups, which are weakly acidic. The siloxane bonds resulting from thermal dehydroxylation through calcination are resistant to subsequent hydrolysis, acquiring a hydrophobic character. The concentration of active silanol groups can be reduced by thermal dehydroxylation above 400 K, being virtually complete at 900 K [62]. Therefore the PZC will vary upon calcination conditions. Moreover, diatomites are not pure silica, therefore the PZC would depend on the amount and nature of its clay components.

The PZC value of the diatomite sample calcined at 700 °C was determined by the mass titration method, reported by Preočanin and Kallay [45]. Subsequent portions of diatomites were added to aqueous solutions (ionic strength 0.004 mol/L) of different initial pH values. The pH of the system changes gradually and approaches a constant value, which is the PZC. Initial pH was adjusted by addition of HNO_3 or KOH. The constant ionic strength of 0.004 mol /L was controlled by KNO_3. The experiments were performed at 25 °C under an N_2 atmosphere. According to results presented in Fig. 7, the point of zero charge is placed between 6–8.

Fig. 6. Mössbauer spectra for the raw material and the samples calcined at 500 °C, 700 °C and 1000 °C.

Table 6
Hyperfine parameters for the studied samples.

Sample	D1		D2		D3		S		
	IS	QS	IS	QS	IS	QS	IS	2εQ	B_hf
Raw	0.38	0.48	0.12	0.59	–	–	–	–	–
500° C	0.31	1.10	–	–	0.49	1.24	–	–	–
700° C	0.37	1.29	0.14	0.58	–	–	[a]	[a]	[a]
1000 °C	0.30	0.86	–	–	–	–	0.38	−0.24	49.4

IS and QS [mm/s], 2εQ: quadrupole shift [mm/s], B_hf: hyperfine magnetic field [T].
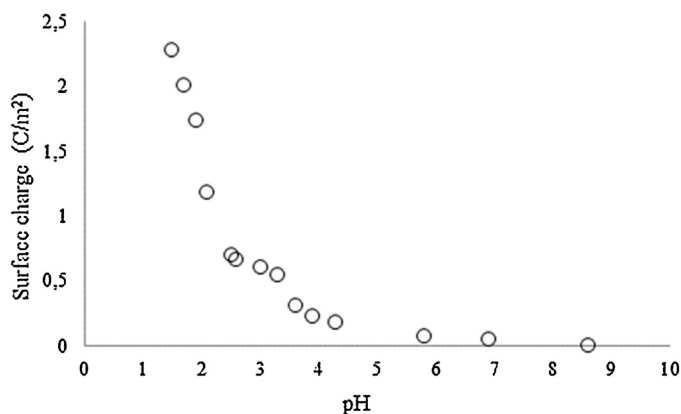
[a] Not fitted but maybe present in scarce content.

Fig. 8. Surface charge of diatomite calcined at 700 °C, determined by the acid titration method.

Fig. 9. Chemical structure of Orange II.

The surface charge was directly determined by the acid titration method [46]. The experiment was performed with an ionic strength of 0.01 mol/L (KCl), with 3 g of the diatomite sample calcined at 700 °C added to 100 mL of twice distilled water. This suspension was titrated with 0.1–1 mol/L HCl. The difference between amounts of acid added to the suspension (electrolyte solution + diatomite) and to a blank solution (without diatomite) gave the net amount of consumed OH^- and H^+. Fig. 8 presents the surface charge curve obtained. From its evolution, a PZC of 8.5 is assumed and therefore, in the pH range studied during the oxidation tests (pH 2–3.5), the surface of diatomite should be positively charged.

3.2. Fenton-like oxidation of Orange II with diatomites

The performance of diatomites as Fenton-like catalyst was tested under several operating conditions. Experiments were performed varying the diatomite calcination temperature (500, 700, 1000 °C), reaction temperature (50, 60, 70, 80 °C); catalyst load (0.47, 0.94, 1.89 and 3.78 g), H_2O_2 dose (10.96, 13.7, 20.55 mmol/L), initial pH (2–3.5) and initial Orange II concentration (100, 200, 500 mg/L).

3.2.1. Preliminary experiments
3.2.1.1. Thermal decomposition. Thermal decomposition of Orange II was evaluated at 70 °C (initial pH 3), in a four hour test. Neither TOC reduction nor decoloration was detected. Moreover, OII (100 mg/L) was oxidized in the absence of catalyst using the stoichiometric amount of H_2O_2 (13.7 mmol/L), at 70 °C and initial pH of 3. A decoloration level of 92% was reached after 4 h; however, the mineralization was negligible. This suggests that only the azo bond was deteriorated but the molecule remained essentially unaltered.

3.2.1.2. Orange II adsorption. Additionally, a previous set of experiments using catalyst without oxidant was performed to discriminate the adsorption effect. A mass of diatomites equivalent to 800 mg/L of Fe in the reaction media was employed, i.e., 4.53 g of diatomites calcined at 500 °C or 3.78 g of diatomites calcined at 700 or 1000 °C. Two temperatures were tested, 50 and 70 °C, starting from pH 3.
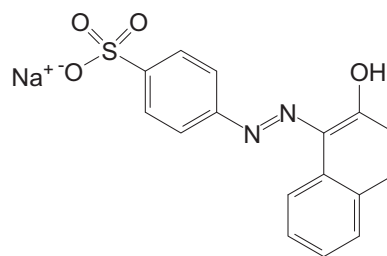
Under those conditions, neither decoloration nor TOC reduction was detected, therefore the adsorption of OII at initial pH 3 was negligible. The OII speciation in solution is given by a pK_a1 of 11.4 for the deprotonation of the naphthalene (OH) and a pK_a2 of 1 for the deprotonation of the SO_3H- group [35]. Fig. 9 shows the chemical structure of OII.

The azo-dye could exist as H_2L (doubly protonated, dominant for pH lower than 1), HL^- (mono protonated, dominant in the pH range between 1 and 10.6), and L_2^- (non-protonated, dominant for pH values greater than 10.6) [63]. Therefore, in the pH range studied in the present contribution, Orange II is monoprotonated (HL^-). In spite of performing the experiments at a pH lower than the PZC, the electrostatic attraction between the positively charged surface and the anionic azo-compound is not sufficient to achieve a noticeable removal of the pollutant. Probably, this could be related to diffusional restrictions [2].

Additional tests were carried out with diatomites calcined at 700 °C, with initial pH of 2, at 50 and 70 °C and with initial pH of 1, at 70 °C. The results are presented in Table 7. As the pH decreases, the positive charge of the surface increases, which favors the adsorption of the anionic dye, which is 90% in the form HL^- and only 10% as HL_2 at pH 2 [64].

3.2.1.3. Diatomite Stability Studies. The stability of diatomites calcined at different temperatures was evaluated by measuring the total carbon (TC) released and the presence of Fe ions in the reaction media. The samples were added to 170 mL of twice distilled water, with initial pH of 3 and agitated during 4 h. Diatomites calcined at 500 °C only released 4 mg/L of TC after 4 h and the pH increased from 3 to 5, due to the protonation of the diatomite surface or the releasing of carbonates. Diatomites calcined at 700 °C released 2 mg/L of TC and the pH increased from 3 to 4. Diatomites calcined at 1000 °C did not released TC and the pH maintained constant. For all samples no iron leaching was detected.

To assess the effect of pH on the diatomites stability, a series of tests was performed by contacting 0.94 g of the sample calcined at 700 °C with 170 mL of twice distilled water at pH 2 and 3, during 4 h. At pH 2, a leaching of 1.3 mg/L was measured at the end though a leaching of 0.5 mg/L was obtained in only 30 min. At pH 3, the loss of iron was negligible.

Additionally, at pH 3, 0.94 g of the sample calcined at 700 °C were contacted with a 100 mg/L solution of oxalic acid, and 60 mg/L solutions of catechol or hydroquinone. These concentrations are higher than the expected in the reaction media during the oxidation tests. Leaching values of 0.4 and 0.2 mg/L were measured in the case

Table 7
OII adsorption at different temperatures and initial pH values.

pH	50 °C		70 °C	
	OII removal (%)	TOC removal (%)	OII removal (%)	TOC removal (%)
1	–	–	31	25
2	24	22	13	12
3	0	0	0	0

of oxalic and catechol, respectively. No leaching was detected in the case of hydroquinone. Therefore, yet low, the leaching of Fe during the oxidation of OII at pH 3 may strongly depend on the product distribution due to iron take-off from the surface during the redox reaction of the oxidizable organic compounds [26].

3.2.2. Peroxidation tests

3.2.2.1. Effect of the calcination temperature.
Oxidation tests were performed at 70 °C with a mass of diatomite equivalent to 800 mg/L of Fe in the reaction media, which is 4.53 g of the diatomites calcined at 500 °C and 3.78 g of diatomites calcined at 700 and 1000 °C. Table 8 summarizes the results.

The performance of the samples calcined at 500 °C or 700 °C was quite similar. Decoloration was completed within the first 30 min of reaction, and the final TOC conversion was around 65%. There were no significant differences between the H_2O_2 conversion rates and the oxidant was completely consumed at the end of the reaction in both cases. The pH increased from 3 to 4, due to the gradual protonation of the silica surface or the release of carbonates.

Samples calcined at 1000 °C presented an induction period probably due to several factors such as diffusional problems, different iron species and diminished initial contribution of homogeneous catalysis. The pH was almost constant. A final TOC value of 54% was obtained.

The calcination temperature did not have an effect in the leaching of Fe, a total cation concentration between 0.6–0.8 mg/L was measured in all cases, which is well below the discharge limits [65].

The diffusional restrictions were evaluated for samples calcined at 700 and 1000 °C. A mass of 3.78 g of the catalyst samples were ground and used in an oxidation test at 70 °C. For both samples the initial rates accelerated; however, final conversions were similar to those obtained with particles of 7–8 mesh (Fig. SD8, Suplementary material).

Samples calcined at 700 °C seemed to be more resistant to attrition and released less TC than samples calcined at 500 °C. Moreover, the surface area reduction during calcination is smaller than in samples calcined at 1000 °C, which would favor the oxidation reaction. Therefore, further experiments were performed with samples calcined at 700 °C.

3.2.2.2. Reaction temperature effect.
The oxidation of OII was evaluated at 50, 60, 70 and 80 °C, with initial pH of 3, adding the stoichiometric demand of H_2O_2. A mass of diatomite equivalent to 800 mg/L of Fe was used (3.78 g). Fig. 10 a–d depicts OII, TOC, H_2O_2 and pH evolution, respectively.

Complete decoloration is achieved after 90 min when the reaction is performed at 50 and 60 °C. At higher temperatures decoloration is almost instantaneous, with a 100% OII conversion after only 30 min of reaction.

At 50 °C, the TOC evolution presents an induction period (60 min), and a final mineralization of 40%. Higher temperatures shorten the induction period. Final TOC conversions of 57, 62 and 52% are obtained at 60, 70 and 80 °C, respectively. At 80 °C, the TOC conversion remains almost constant after the first 60 min, which could be related to the fast H_2O_2 depletion. Complete oxidant consumption is obtained after 60 min due to the parasitic decomposition of H_2O_2 into H_2O and O_2, promoted at higher temperatures [33,66].

According to the results presented in Table 8 the optimum temperature in terms of hydrogen peroxide consumption efficiency is 70 °C. At 80 °C the thermal decomposition of the oxidant results in a higher H_2O_2 consumption with a lower TOC reduction.

The detrimental effect of temperature has been sometimes proposed for homogeneous Fenton but there are strong evidences showing that high temperature can be beneficial in heterogeneous Fenton [49].

Table 8
Final pH and OII, TOC and H_2O_2 final conversions (240 min) under the whole operating conditions studied.

| Calcination T (°C)	Reaction T (°C)	Catalyst (g)	H_2O_2 (mmol/L)	OII (mg/L)	Initial pH	X_{OII}	X_{TOC}	X_{H2O2}	Final pH	Leaching (%)	η	ϵ
500	70	4.53	13.7	100	3	100	65 ± 5	100 ± 0.3	4 ± 0.6	0.8 ± 0.3	75.5	75.5
700	70	3.78	13.7	100	3	100	62 ± 5	100 ± 0.5	3.7 ± 0.2	0.6 ± 0.2	72	72
1000	70	3.78	13.7	100	3	100	54 ± 4	95 ± 6	3 ± 0.5	0.8 ± 0.3	66	63
700	50	3.78	13.7	100	3	100	40 ± 6	74 ± 5	3.55 ± 0.2	0.9 ± 0.3	63	46.5
700	50	0.94	13.7	100	3	100	36 ± 5	74 ± 6	3.3 ± 0.2	0.9 ± 0.3	56.5	42
700	60	3.78	13.7	100	3	100	57 ± 1.8	92.3 ± 4	3.75 ± 0.4	0.6 ± 0.1	72	66
700	80	3.78	13.7	100	3	100	53 ± 7	100 ± 0.5	3.9 ± 0.2	0.5 ± 0.3	62	61.5
700	50	3.78	13.7	100	2	100	50 ± 2	100 ± 1	2.6 ± 0.2	–	58	58
700	70	3.78	13.7	100	2	100	53 ± 8	100 ± 1	2.7 ± 0.4	15 ± 1	62	61.5
700	70	3.78	13.7	100	3.5	100	10 ± 5	65 ± 2	4.7 ± 0.2	0.6 ± 0.3	18	11.6
700	50	3.78	13.7	100	3.3	100	10.3 ± 5	33 ± 7	3.1 ± 0.3	0.8 ± 0.2	36.3	12
700	70	0.47	13.7	100	3	100	62 ± 1.4	77 ± 7	3.1 ± 0.2	0.6	94	72
700	70	0.94	13.7	100	3	100	67 ± 3	90.4 ± 6	3.6 ± 0.2	0.7 ± 0.2	86	78
700	70	1.89	13.7	100	3	100	68 ± 3	94 ± 5	3.6 ± 0.2	1.3 ± 1	84	79
700	70	0.94	11.0	100	3	100	66 ± 2	100 ± 1	3.4 ± 0.1	0.8 ± 0.3	77	76.7
700	70	0.94	20.6	100	3	100	68 ± 5	73 ± 5	3.3 ± 0.1	0.7 ± 0.3	77	79
700	70	3.78	27.4	200	3	100	66 ± 5	100 ± 4	3.8 ± 0.2	0.9 ± 0.3	108.2	153.4
700	70	3.78	68.5	500	3	100	71 ± 0.1	92 ± 4	3.6 ± 0.4	3 ± 0.3	90	412.5
700	70	0.94	68.5	500	3	100	61 ± 5	51 ± 4	3 ± 0.1	2.7 ± 0.5	139	354.4
700	70	3.78	68.5	OII ± NaCl	3	100	61 ± 1.7	87 ± 4	3.5 ± 0.4	2.3 ± 0.5	81.5	354.4
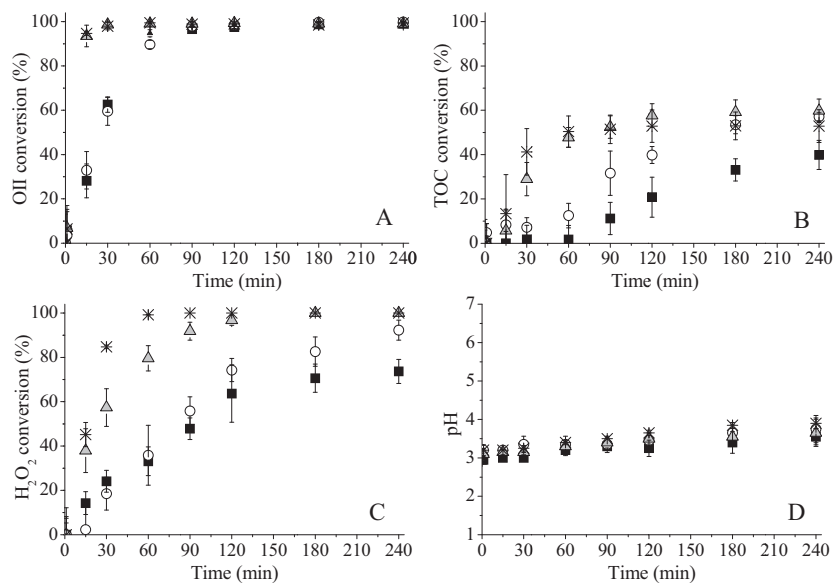
Fig. 10. Conversions of (a) OII, (b) TOC, (c) H_2O_2, and (d) pH evolution as a function of time at different temperatures (■) 50 °C; (○) 60 °C; (△) 70 °C, (✳) 80 °C. Other experimental conditions: $[OII]_0 = 100$ mg/L, load of diatomite = 3.78 g, $[H_2O_2]_0 = 13.7$ mmol/L, $pH_0 = 3.0$.

The pH slightly rises due to the protonation of the diatomite surface or the releasing of carbonates. In spite of the formation of HNO_3 and $NaHSO_4$ from the mineralization of OII, the concentration of these acids would be relatively low compared to the high H^+ concentration (initial pH 3), having nil effect on the solution pH.

The induction period observed during mineralization could be due to several causes. Some researchers have suggested a surface activation, such as the protonation of the surface iron species, since it was observed that a lower pH shortened the induction time [67,68]. Others relate it to the adsorption of the reactants onto the catalyst surface or to the time needed to dissolve enough iron for the homogeneous Fenton reaction to take place [67,69]. In our case, it was detected a leaching of 0.33 mg/L after the first 30 min of reaction, at 70 °C. Meanwhile, the Fe leached after 30 min, at 50 °C was negligible. This could explain the much longer induction period at lower temperatures. Moreover, the contribution or activity of a small amount of iron in the reaction solution would be less important at lower temperatures. According to the stability tests the leaching is associated to the presence of different reaction intermediates, such as quinones or carboxylic acids. The initial catalytic process is a heterogeneous phenomenon and the preliminary aromatic intermediates have complexing properties, which could cause the removal of iron from the surface of the catalyst. These quinone compounds are rapidly formed at 70 °C through the heterogeneous process and then an early leaching of iron occurs, promoting the occurrence of the homogeneous Fenton reaction, which would reduce the induction period.

This lag period has also been associated to the proportion of Fe(II)/Fe(III). A higher amount of Fe(II) diminish the reaction delay. It has been reported that quinone and quinone-like compounds such as hydroquinone or catechol function as reducing agents for Fe(III), promoting the Fenton reaction [70–73]. Therefore, the fast occurrence of these intermediates at 70 °C could also reduce the induction period.

Fig. 11 shows the UV–vis spectrum of the reaction media at different times, when the oxidation is performed at 70 °C. Orange II has three absorption peaks at 230, 312 and 485 nm. The wavelength of its visible absorption peak is 485 nm and it corresponds to the chromophore containing azo linkage. The absorption peaks in the UV region at 230 nm and 312 nm are assigned to the benzene ring and naphthalene ring [32,33]. At the end of the test, there is no signifi-

cant absorbance in the visible region, indicating that color removal was practically completed (breakdown in the chromophore group). However, the spectrum in the UV region shows that the dye was not mineralized completely, though the absorption was reduced over the UV range.

Several studies have reported the intermediates identified during the oxidation of Orange II [30,33,41] which included HSO_4^-, NH_4^+, and NO_3^-, 4-hydroxybenzenesulfonic acid, nitrogen and sulfo- containing products, benzenesulfonate, carboxylic and dicarboxylic acids (phthalic, succinic, maleic, malonic, acetic, oxalic, formic acids) and their anions [30–33]. However, none of these compounds absorb in the visible region, indicating that the absorbance decrease at 485 nm is only due to the dye degradation [30–33]. The mineralization products reported are nitrite, nitrate, sulfate, and CO_2.

3.2.2.3. Initial pH effect. The initial pH effect was evaluated at 50 °C and 70 °C, with a catalyst load of 3.78 g and the stoichiometric amount of H_2O_2. The results are presented in Table 8.

Two experiments were performed at 50 °C with only a slight variation of the pH. The first test started with a pH of 3 and the second test with a pH of 3.3. The pH in the reaction media increased gradually because of the protonation of hydroxyl groups in the sur-
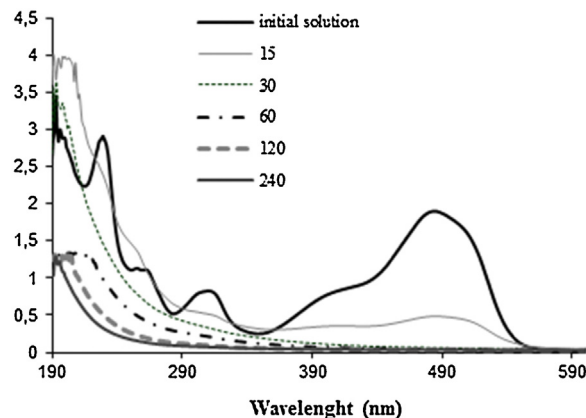

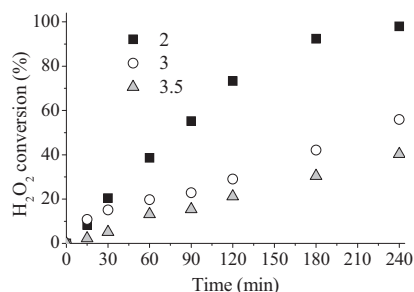**Fig. 11.** Reaction media spectra at different reaction times.

Fig. 12. H_2O_2 decomposition in absence of OII at different initial pH values (2, 3, 3.5).

face of diatomite and the releasing of carbonates. The pH in the first reaction was close to 3.3 during the first hours. The pH in the second reaction maintained around 3.5. Several tests were also performed at 70 °C, with initial pH values of 2, 3 and 3.5.

It can be noted that a small variation in the pH has a great impact on the oxidation performance, especially at 50 °C, where the decoloration is drastically decelerated, reaching 93 % after 240 min with the highest pH and 95% in 60 min with the lowest pH. Moreover, when the initial pH is increased, the final mineralization decreases from 40 to 10%. It was also observed that the mineralization level can be increased up to 50% if the pH is drastically reduced up to 2.

Tests carried out at 70 °C with pH values higher than 3.5 reached decoloration levels around 75%. On the contrary, the mineralization was negligible.

These results are related to the stability of H_2O_2 which is affected by the pH [30]. At higher pH values, the rapid H_2O_2 decomposition produces molecular oxygen without formation of appreciable amounts of hydroxyl radicals [30,33]. Moreover, as pointed out by Buxton et al. [74], the oxidation potential of $OH^\bullet$ decreases at higher pH. While this value ranges between 2.65 to 2.80 V at pH 3.0, it lowers to 1.90 V at pH 7.0 [74,75]

In order to assess the effect of pH in the decomposition of H_2O_2, several tests were carried out at 70 °C, in the absence of OII, with 0.94 g of catalyst, initial H_2O_2 concentration of 13.7 mmol/L and different initial pH values (2, 3, and 3.5). Fig. 12 presents the hydrogen peroxide decomposition evolution under different pH values.

According to these results, the H_2O_2 decomposition is decelerated with increasing pH values. Some authors ascribe this phenomenon to the surface activation through protonation in a non-radical mechanism of reaction [76]. According to the mechanism proposed by Andreozzi et al. [76] for the peroxidation of ferulic acid, the disappearance of this substrate is the result of the reaction between the dissolved acid and the H_2O_2 adsorbed in the surface.

Considering that iron oxides are the active sites, which can assume different forms according to the pH, the $Fe-OH_2^+$ will prevail at low pH whereas the $Fe-O^-$ form will dominate at high pH. Then the $Fe-OH_2^+$ form would be responsible for the H_2O_2 adsorption [76]:

$$-M-OH_2^+ \ + \ H_2O_2 \ \leftrightarrow \ H_2O \ + \ -M-O-OH$$
$$\underset{H}{\overset{\uparrow}{}}$$
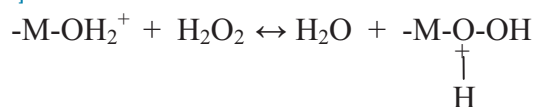
It is also worth to notice that the H_2O_2 consumption is higher in the presence of OII, which could be connected to the leaching of iron under these conditions. In the absence of OII, at pH 3 or higher, the catalyst does not leach Fe, while at pH 2 a leaching of 1.6 mg/L is detected at the end of the test. During the OII oxidation tests, at pH 3, a leaching of 0.6 mg/L was detected after 60 min of reaction and, at pH 2, a leaching of 5.2 mg/L was measured after only 15 min. In

the presence of OII, the loss of Fe is impelled due to the complexing action of the oxidation intermediates, such as oxalic acid [26].

Moreover, as mentioned above, it has been reported that the presence of certain reductive intermediates, such as hydroquinone or catechol, play an important role in the Fenton mechanism [77]. Therefore, these intermediates could accelerate the H_2O_2 decomposition during the oxidation of OII.

What is more, at pH > 3, there is no adsorption of Orange II (see Section 3.2.1.2). Therefore, the decoloration of the dye mainly owns to degradation. At pH 2, the diatomite surface turns more positive and the electrostatic attraction between dye molecules and the diatomite surface increases. At pH 2, the decoloration is almost immediate and the initial mineralization rate is higher. The increase of the adsorbed dye together with a higher homogeneous contribution (5.2 mg/L of Fe after 15 min) would lead to a higher degradation rate. Nevertheless, as the oxidant is completely consumed too early in the reaction (in only 30 min), the mineralization level reached (51%) is lower than that obtained (62%) with initial pH 3.

Therefore, according to the oxidation and leaching results, the optimal pH for reaction in this catalytic system would be 3. This agrees with several previous studies that also found an optimal pH of 3 for the degradation of OII [30,33,42,78].

3.2.2.4. Catalyst concentration effect. The catalyst load effect was evaluated at 70 °C, with the stoichiometric demand of H_2O_2, initial pH of 3 and with a catalyst concentration equivalent to 100, 200, 400 and 800 mg/L of Fe, which is 0.47, 0.94, 1.89 and 3.78 g of diatomite, respectively. Fig. 13a–d presents the results obtained.

The evolution of OII and TOC resulted quite similar for reactions performed with 0.94, 1.89 and 3.78 g of diatomite. Complete decoloration was achieved after 60 min of reaction for all catalyst loads studied. The final TOC values are slightly lower (62%) for the reaction performed with the highest catalyst concentration (3.78 g of diatomite). This could be due to the parasitic reactions promoted by the excess of catalyst [32,33,79,80]. In this case, the TOC conversion maintained almost constant after the first two hours of reaction, which is related to the H_2O_2 evolution; the oxidant was almost consumed after 120 min. The H_2O_2 decomposition increased with larger catalyst concentrations as pointed out by several authors [33,80,81].

The pH was almost constant when smaller amounts of catalyst were used (0.47 and 0.94 g). With higher catalyst concentrations, the pH increased from 3 to 3.6–4, due to the higher surface area available for protonation and liberation of carbonates.

With catalyst loads higher than 0.94 g, a TOC conversion of 60% was achieved after 120 min, with a final mineralization of almost 70%. With the lowest catalyst concentration (0.47 g of diatomite), the TOC conversion evolution rate resulted much lower, showing a mineralization of 40% after 120 min and a final TOC conversion of 61%. Considering the higher mineralization level, the optimal catalyst load under this operating conditions resulted 0.94 g.

3.2.2.5. Effect of the oxidant dose. The initial H_2O_2 concentration (10.96, 13.7 and 20.55 mmol/L) was evaluated at 70 °C with a catalyst load of 0.94 g (equivalent to 200 mg/L of Fe) and initial pH of 3. Results are presented in Table 8. No differences were observed in the oxidation rates or final TOC or OII conversions. This could be due to the formation of recalcitrant final intermediates. Moreover, it should be noted, that the TOC conversions obtained after 240 min, under the whole operating conditions evaluated in this study, do not achieve values above 70%. Only after 6 h of reaction the mineralization level slightly rises up to 74%. One more test was performed with two equal doses of H_2O_2, one at the beginning of the reaction and the second one added at 240 min. The dose corresponded in both cases to the initial stoichiometric demand. After
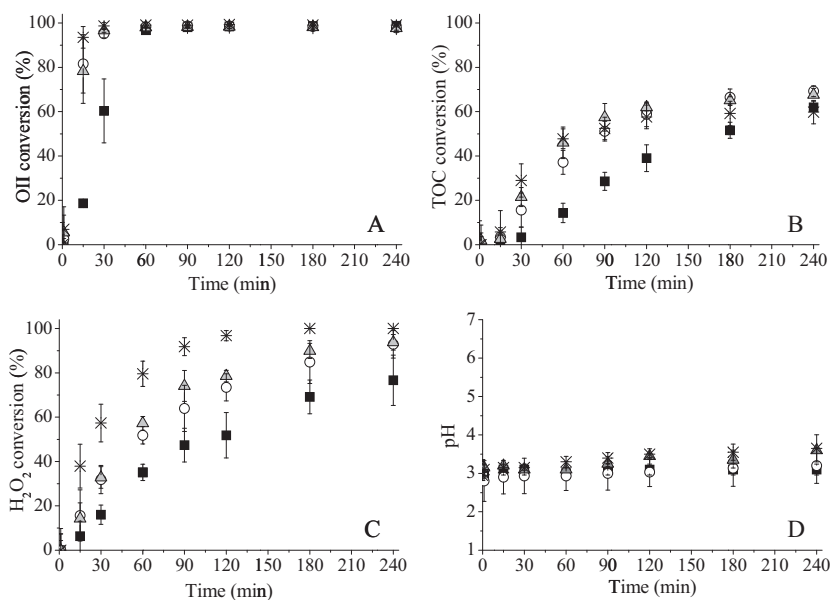
Fig. 13. Conversions of (a) OII, (b) TOC, (c) H_2O_2, and (d) pH evolution as a function of time with different catalyst loads (■) 0.47; (◯) 0.94; (△) 1.89, (✳) 3.78 g. Other experimental conditions: $[OII]_0 = 100$ mg/L, $[H_2O_2]_0 = 13.7$ mmol/L, $pH_0 = 3$, $T = 70\,°C$.

6 h a TOC conversion of 74% was obtained, the same value achieved without the second H_2O_2 dose.

3.2.2.6. Effect of the OII concentration. The performance of the catalyst was evaluated at 70 °C using higher OII concentrations, i.e. 0.57 and 1.43 mmol/L (200–500 mg/L). In each test, the stoichiometric amount of H_2O_2 was added. The results are presented in Table 8. The results obtained were quite positive; the catalyst was able to mineralize 60–70% of the pollutant, in the whole concentration range studied. In order to obtain higher mineralization levels it was necessary to increase the diatomite load from 0.94 to 3.78 g (800 mg/L Fe)

The leaching of iron increased with higher OII concentrations. Iron concentrations of 0.6, 0.8 and 3 mg/L were measured for reactions performed with 100, 200 and 500 mg/L of OII, respectively. The presence of a higher concentration of certain final intermediates, such as oxalic acid, could increase the leaching of iron by complexation [26].

3.2.2.7. Scavenging effect of NaCl in the Fenton reaction. The inhibitive effect of chloride on the Fenton reaction has repeatedly been reported by several authors [82,83] and it is associated to the following reactions:

$$Cl^- + {}^\bullet OH \rightarrow Cl^\bullet + OH^-$$

$$Cl^- + Cl^\bullet \rightarrow Cl_2 + e^-$$
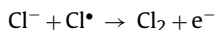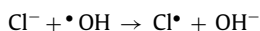
The oxidation potential of chlorine (1.36 V) is much lower than that of hydroxyl radicals (2.8 V).

With the purpose of studying the behavior of the catalyst under more realistic conditions, the scavenging effect of NaCl was evaluated, as it is a compound commonly present in the dying bath. The aqueous solution consisted of 1.43 mmol/L (500 mg/L) of Orange II and 12,500 mg/L of NaCl (0.2 mol/L). A catalyst concentration of 3.78 g was employed. Results are shown in Table 8. The oxidation reaction is decelerated due to the scavenging effect of chloride ion. However, decoloration is completed and the mineralization level achieved is still acceptable (61%).

3.2.2.8. Catalyst stability. In order to evaluate the long term stability of the catalyst a mass of 0.94 g (corresponding to 200 mg/L of Fe) was retained and used again in successive runs at 70 °C, with 0.28 mmol/L (100 mg/L) of OII, initial pH 3, using the stoichiometric demand of H_2O_2 and without treatment of the diatomite sample between tests. The catalyst was used in five consecutive oxidation reactions of four hours each. Fig. 14 shows the OII and TOC evolution during the first and fifth run. According to the results, the stability of the catalyst maintains after 20 h of usage, with a final Fe loss of 2.25%. An average of 0.88 mg/L of iron leached after each run. Also, in order to evaluate the contribution of the iron catalytic sites in the diatomite sample, a mass of 5 g of the sample calcined at 700 °C was treated during 3 h with 100 mL of HNO_3 (65%) at 80 °C, under reflux, in a controlled temperature silicone oil bath. The labile iron present in the sample was extracted and the final percentage of the cation was reduced from 3.6 to 3.16%. The BET area increased from 76 m^2/g to 119 m^2/g. The acid dissolved the inorganic matter and opened up microscopic porosities, now accessible for N_2 during BET operation [50]. This sample was washed with distilled water until neutral pH, dry and finally use in an oxidation test to evaluate the catalytic behavior of the remnant iron. A mass of 4.3 g equivalent to 800 mg/L of Fe in the OII solution was employed. The reaction
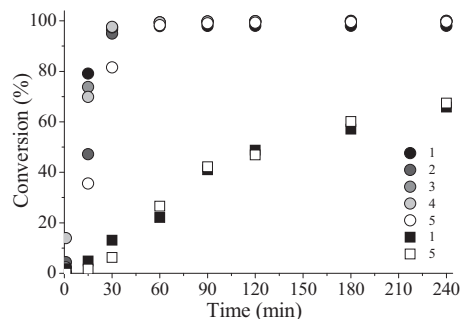

Fig. 14. TOC and OII evolution during successive runs (70 °C, 0.94 g of diatomites), squares and circles correspond to TOC and OII conversion values, respectively.
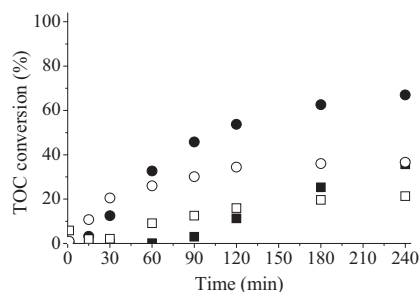
Fig. 15. TOC conversion evolution for the heterogeneous reactions with 0.94 g of diatomites (full symbols) and the homogeneous contribution of 0.7 mg/L of Fe(II) (open symbols), at 50 °C (squares) and 70 °C (circles).

was carried out at 70 °C, during 4 h, with 0.28 mmol/L of OII and the stoichiometric amount of H_2O_2.

In spite of the high percentage of iron still present in the diatomite (3.16%), the TOC conversion dropped from 62% with the original sample to 47% with the acid treated sample. This means that even though there is a high percentage of iron in the diatomite, it is not all equally available or active in the Fenton process. The EDX analysis of the acid treated sample (see Table SD1 in the Supplementary material) shows that the percentage of iron in the surface (1.9%) is lower than in the core of the catalyst (3.3%). The final leaching measured was 0.13 mg/L. This could be related to the stronger bonding of the iron not extracted during the HNO_3 treatment. Moreover, the removal of the labile iron diminished the homogeneous contribution, which is related to the lower TOC conversion values.

3.2.2.9. Homogeneous contribution. As it was discussed in Section 3.2.1.3, the loss of iron ions from the surface of the catalyst may be attributed to the presence of complexing reaction intermediates. The released aqueous Fe^{2+} could contribute to the OII degradation by a conventional homogeneous Fenton reaction step. The homogeneous contribution was evaluated at 50 °C and 70 °C, with 0.28 mmol/L of OII, stoichiometric requirement of H_2O_2 and 0.7 mg/L of Fe^{2+}. TOC results are presented in Fig. 15.

In the homogeneous system decoloration is completed in 15 min at 70 °C and in 90 min at 50 °C. However, the TOC conversion does not reach the mineralization level achieved by the heterogeneous catalyst. Taking into account that the activity obtained under the heterogeneous conditions was higher than the activity shown in the homogeneous reaction, the mineralization occurs predominantly as a result of the reaction between the H_2O_2 and the iron oxide present in the diatomite.

3.2.2.10. Adsorption of reaction intermediates. The effect of the catalyst concentration was evaluated (Fig. 13a–d) and an increment beyond a catalyst load of 0.94 g did not affect the TOC removal results. This could be a sign of the low sorption capacity of the material. In addition, according to the stability tests, the activity of the catalyst is not affected by the possibly adsorbed intermediates, since its usage in successive runs yielded the same results.

The appearance and disappearance of several peaks in the UV–vis spectra indicate that this is not a purely sorption process, the catalytic oxidation of the azo-dye and intermediates occurs as well. However, some intermediates could be adsorbed in the diatomite surface. Thermogravimetric analysis (TGA) was performed to confirm the existence of adsorbed compounds. Data were captured using a TGA (Shimadzu, model TGA-50) instrument with a constant airflow of 20 mL/min. The heating rate applied was 10 °C/min and the temperature was increased from 25 °C to 900 °C. However, the temperature was first kept constant at 110 °C for 30 min in order to assure the complete removal of water contained in the sample.

The TGA analysis was performed using a fresh sample and a catalyst sample (0.94 g) used in 1 or 5 consecutive cycles, at 70 °C (see Fig. SD9 and SD10 in the Supplementary material). The TGA results obtained with the sample used in only one test show no differences with the results obtained with the fresh sample. According to the TGA of the sample used in 5 consecutive reactions, 1% of the weight loss could be related to the sorption of reaction intermediates. As the exact nature of the adsorbed compounds can hardly be assessed, their equivalence in terms of TOC cannot be conducted. In opposition to the results obtained after only one usage, the catalyst employed in several tests shows an increment in its sorption capacity which is related to its higher surface area.

Desorption tests were performed placing samples used in one or five consecutive tests (0.94 g or 3.78 g) in 170 mL of bidistilled water at pH 11.5 and 70 °C (initial TC of 3 mg/L). This pH is much higher than the point of zero charge of the diatomite (PZC 6–7) and therefore a change of the catalyst surface charge, from positive to negative, is expected, which could cause the releasing of the adsorbed compounds. The same test was also performed with a fresh catalyst sample. No differences were detected; a total carbon concentration (TC) around 5 mg/L was measured in all cases (see Table SD2 in the Supplementary material). These results may indicate low sorption capacity under the operating conditions studied and therefore, the differences between the heterogeneous and homogeneous processes (Section 3.2.2.9) would not be attributed to the removal of the intermediate compounds through adsorption.

4. Conclusions

Calcined diatomite samples (3.5% Fe content) were employed as Fenton-like catalysts for the degradation of Orange II solutions (0.28–1.43 mmol/L) at various operating conditions.

Different characterization techniques indicated the presence of an amorphous silica phase, characteristic of the diatom frustules and important amount of clay minerals, specially nontronite, iron rich member of the smectite family. All the iron presented in the sample was as Fe^{3+} and the octahedral Fe seemed to be in an environment somewhat similar to that of nontronite. The sample calcined at 700 °C presented more resistance to attrition, with a high surface area of 76 m²/g and a half pore width of 3.7 nm.

At 70 °C, initial pH 3, and using the stoichiometric amount of H_2O_2, complete decoloration, TOC reduction close to 67% and a negligible Fe leaching were achieved with samples calcined at 700 °C. Under these conditions, no adsorption was detected so the OII removal was mainly due to degradation. The activity obtained under the heterogeneous conditions was higher than the homogeneous activity shown by the iron leached. Therefore, the oxidation mechanism was mostly heterogeneous.

Under more drastic conditions (500 mg/L of OII), the catalyst still yielded high levels of mineralization, although the iron leached increased due to the take-off from the surface by a higher concentration of reaction intermediates possessing complexing properties. The presence of a high concentration of NaCl decelerated the oxidation reaction due to its scavenging effect. However, the mineralization level reached was still acceptable.

The catalyst used in consecutive runs (up to 20 h) yielded similar performance in terms of decoloration and TOC reduction. The leaching of iron was below the discharge limits in most cases (0.6-0.8 mg/L).

Overall, this study added to the characterization of this extremely cheap, ecofriendly material, used as catalyst in Fenton-like wastewater treatment. Its performance was comparable or even better than data reported in literature using more complex and expensive catalysts and less concentrated solutions.

Acknowledgements

Appendix A. Supplementary data

Supplementary data associated with this article can be found, in the online version, at http://dx.doi.org/10.1016/j.apcatb.2015.08.022.

References

[1] B. Bahramian, F.D. Ardejani, V. Mirkhani, K. Badii, Appl. Catal. A Gen. 345 (1) (2008) 97–103.
[2] M.A.M. Khraisheh, S.J. Al-Ghouti, M.N. Ahmad, Water Res. 39 (5) (2005) 922–932.
[3] H. Mahanni, M. Kasemeini, Sci. Iran. 10 (2003) 350–356.
[4] M. Al-Ghouti, M.A.M. Khraisheh, M.N.M. Ahmad, S. Allen, J. Colloid Interface Sci. 287 (1) (2015) 6–13.
[5] Z. Ge-shan, X.U.E. Hong- hai, T. Xiao-jian, P. Fei, K. Chun-li, Chem. Res. Chin. Univ. 27 (6) (2011) 1035–1040.
[6] H. Elden, G. Morsy, M. Bakr, Asian J. Mat. Sci. 2 (3) (2010) 121–136.
[7] R.A. Shawabkeh, M.F. Tutunji, Appl. Clay Sci. 24 (2003) 111–120.
[8] M. Koyuncu, Physicochem. Probl. Miner. Process. 48 (2) (2012) 485–494.
[9] M. Šljivić, I. Smičiklas, S. Pejanović, I. Plećaš, Appl. Clay Sci. 43 (2009) 33–40.
[10] M. Khraisheh, Y. Aldegs, W. Mcminn, Chem. Eng. J. 99 (2) (2004) 177–184.
[11] H. Mohamedbakr, M. Burkitbaev, Open Mineral. J. 3 (2009) 12–16.
[12] P. Moslehi, P. Nahid, IJE Trans. B Appl. 20 (2) (2007) 141.
[13] R. Knoerr, J. Brendlé, B. Lebeau, H. Demais, Microporous Mesoporous Mater. 169 (2013) 185–191.
[14] P. Banković, M. Stanković, P. Tzvetkov, R. Edreva-Kardjieva, M. Shopska, J. Krstić, T.D. Jovanović, M. Gabrovska, J. Mol. Catal. A Chem. 297 (1) (2009) 54–62.
[15] E. Nino, A. Lapena, J. Martinez, J.M. Gutierrez, S. Mendioroz, J.L.G. Fierro, J.A. Pajares, Stud. Surf. Sci. Catal. 16 (1983) 747–755.
[16] I. Puskas, B.L. Meyers, J.B. Hall, Catal. Today 21 (1994) 243–251.
[17] Q. Zhu, Y. Zhang, F. Zhou, F. Lv, Z. Ye, F. Fan, P.K. Chu, Chem. Eng. J. 171 (1) (2011) 61–68.
[18] C. Z. Sun, S. Bai, X. Zheng, R.L. Frost Yang, Appl. Catal. A Gen. 458 (103) (2013) 110.
[19] C. Wang, H. Liu, Z. Sun, J. Huang, Y. Liao, International Journal of Photoenergy (2015), http://dx.doi.org/10.1155/2012/689807.
[20] H. Liu, G. Lu, Y. Guo, Y. Guo, J. Wang, Chem. Eng. J. 108 (3) (2005) 187–192.
[21] W. Y. Jia, G. Han, W. Yang Xiong, Sci. Technol. Adv. Mater 8 (1–2) (2007) 106.
[22] E. Garrido-Ramírez, B.K.G. Theng, M.L. Mora, Appl. Clay Sci. 47 (3–4) (2010) 182–192.
[23] S. Navalon, M. Alvaro, H. Garcia, Appl. Catal. B Environ 99 (12) (2010) 1–26.
[24] C.B. Molina, J.A. Casas, A.H. Pizarro, J.J. Rodriguez, Pillared Clays as Green Chemistry Catalysts: Application to Wastewater Treatment, in: J.P. Humphrey, D.E. Boyd (Eds.), Nova Science Publishers, Inc, 2011, 2015, pp. 435–474.
[25] S.-S. Lin, M.D. Gurol, Environ. Sci. Technol. 32 (1998) 1417–1423.
[26] L.-T. Pham, C. Lee, F.M. Doyle, D.L. Sedlak, Environ. Sci. Technol. 43 (2009) 8930–8935.
[27] L.-T. Pham, F.M. Doyle, D.L. Sedlak, Water Res. 46 (2012) 6454–6462.
[28] G. Centi, S. Perathoner, Catal. Today 77 (4) (2003) 287–297.
[29] J.H. Ramírez, F.M. Duarte, F.G. Martins, C.A. Costa, L.M. Madeira, Chem. Eng. J. 148 (2009) 394–404.
[30] J.H. Ramírez, C.A. Costa, L.M. Madeira, G. Mata, M.A. Vicente, M.L. Rojas-Cervantes, A.J. López- Peinado, R.M. Martín-Aranda, Appl. Catal. B Environ. 71 (1–2) (2007) 44–56.
[31] J.H. Ramírez, M. Lampinen, M.A. Vicente, C.A. Costa, L.M. Madeira, Ind. Eng. Chem. Res. 47 (2008) 284–294.
[32] J.H. Ramírez, C.A. Costa, L.M. Madeira, Catal. Today 107–108 (2005) 68–76.
[33] J.H. Ramírez, F.J. Maldonado-Hódar, a. F. Pérez-Cadenas, C. Moreno-Castilla, C. a. Costa, L.M. Madeira, Appl. Catal. B Environ. 75 (3–4) (2007) 312–323.
[34] F. Duarte, F.J. Maldonado- Hódar, A.F. Pérez- Cadenas, L.M. Madeira, Appl. Catal. B Environ. 85 (2009) 139–147.
[35] X. Liang, Y. Zhong, S. Zhu, J. Zhu, P. Yuan, H. He, J. Zhang, J. Hazard. Mater. 181 (1–3) (2010) 112–120.
[36] S. Nam, V. Renganathan, P.G. Tratnyek, Chemosphere 45 (2001) 59–65.
[37] B. Lodha, S. Chaudhari, J. Hazard. Mater. 148 (1–2) (2007) 459–466.
[38] F. Duarte, F.J. Maldonado-Hódar, L.M. Madeira, Appl. Catal. B Environ. 103 (1–2) (2011) 109–115.
[39] J. Deng, J. Jiang, Y. Zhang, X. Lin, C. Du, Y. Xiong, Appl. Catal. B Environ. 84 (2008) 468–473.
[40] B.-H. Moon, Y.-B. Park, K.-H. Park, Desalination 268 (1–3) (2011) 249–252.
[41] N. Chahbane, D.-L. Popescu, D. a. Mitchell, A. Chanda, D. Lenoir, A.D. Ryabov, K.-W. Schramm, T.J. Collins, Green Chem. 9 (2007) 49–57.
[42] L. Chen, C. Deng, F. Wu, N. Deng, Desalination 281 (2011) 306–311.
[43] E. Ember, S. Rothbart, R. Puchta, R. van Eldik, New J. Chem. 33 (2009) 34–49.
[44] R.A. Brand, Normos program, International Report, Angewandte Physik, Univ, Duisburg, 1987.
[45] T. Preočanin, N. Kallay, Croat. Chem. Acta 71 (4) (1998) 1117–1125.
[46] M. Tschapek, L. Tcheichvili, C. Wasowski, Clay Miner. 10 (1974) 219–229.
[47] H. Zhang, H. Fu, D. Zhang, J. Hazard. Mater. 172 (2009) 654–660.
[48] E. Bolova, G. Gunduz, M. Dukkanci, Int. J. Chem. Reactor Eng. 10 (A18) (2013) 1–21.
[49] J.A. Zazo, G. Pliego, S. Blasco, J.A. Casas, J.J. Rodríguez, Ind. Eng. Chem. Res. 50 (2011) 866–870.
[50] A. Chaisena, K. Rangsriwatananon, J. Sci. Technol. 11 (2004) 289–299.
[51] S.S. Ibrahim, A.Q. Selim, J. Ore Dressing 12 (23) (2010) 24–32.
[52] S.S. Ibrahim, A.Q. Selim, Physicochem. Probl. Miner. Process. 48 (2) (2012) 413–424.
[53] N. Ediz, I. Bentli, I. Tatar, Int. J. Miner. Process. 94 (2010) 129–134.
[54] B.A. Goodman, J.D. Russell, A.R. Fraser, F.W.D. Woodhams, Clays Clay Miner. 24 (1976) 53–59.
[55] I. Rozenson, L. Heller- Kallai, Clays Clay Miner. 25 (1977) 94–101.
[56] J.M.D. Coey, At. Energy Rev. 18 (1980) 73–124.
[57] L. Heller-Kallai, I. Rosenson, Phys. Chem. Miner. 7 (1981) 223–238.
[58] D. Bonnin, G. Calas, H. Suquet, H. Pezerat, Phys. Citem. Miner. 12 (1985) 55–64.
[59] A. Decarreau, F. Colin, A. Herbillon, A. Manceau, D. Nahon, H. Paquet, D. Trauth- Badaud, J.J. Trescases, Clays Clay Miner. 5 (1) (1987) 1–10.
[60] A. Manceau, V.A. Drits, B. Lanson, D. Chateigner, J. Wu, D. Huo, W.P. Gates, J.W. Stucki, Am. Miner. 85 (2000) 153.
[61] M.A. Al-Ghouti, M.A.M. Khraisheh, S.J. Allen, M.N. Ahmad, J. Environ. Manage. 69 (2003) 229–238.
[62] C. Kemball, D.A. Dowden, G.J.K. Acres, A.J. Bird, J.W. Jenkins, F. King, Catalysis 4 (1981) 1–30.
[63] L. Abramian, H. El- Rassy, Chem. Eng. J. 150 (2–3) (2009) 403–410.
[64] J. Bandara, J.A. Mielczarski, J. Kiwi, Langmuir 15 (1999) 7670–7679.
[65] M. Hartmann, S. Kullmann, H. Keller, J. Mater. Chem. 20 (2010) 9002–9017.
[66] J.L. Sotelo, G. Ovejero, F. Martínez, J.A. Melero, A. Milieni, Appl. Catal. B Environ. 47 (2004) 281–294.
[67] M. Luo, D. Bowden, P. Brimblecombe, Appl. Catal. B Environ. 85 (2009) 201–206.
[68] L. Xu, J. Wang, J. Hazard. Mater. 186 (2011) 256–264.
[69] F.V.F. Araujo, L. Yokoyama, L.A.C. Teixeira, J.C. Campos, Braz. J. Chem. Eng. 8 (4) (2011) 605–616.
[70] J. Maekawa, K. Mae, H. Nakagawa, J. Environ. Chem. Eng. 2 (2014) 1275–1280.
[71] Y. Du, M. Zhou, L. Lei, J. Hazard Mater. 136 (3) (2006) 859–865.
[72] A.F. Bautista, J.A. Casas, J.A. Zazo, J.J. Rodriguez, J. Chem. Technol. Biotechnol 86 (4) (2011) 497–504.
[73] C. di Luca, F. Ivorra, P. Massa, R. Fenoglio, Ind. Eng. Chem. 51 (2012) 8979–8984.
[74] G.V. Buxton, C.L. Greenstock, W.P. Helman, A.B. Ross, J. Phys. Chem. Ref. Data 17 (2) (1988) 513–886.
[75] A.A. Burbano, D.D. Dionysiou, M.T. Suidan, T.L. Richardson, Water Res. 39 (2005) 107–118.
[76] R. Andreozzi, M. Canterino, V. Caprio, I. Di Somma, R. Marotta, J. Hazard. Mater. 152 (2008) 870–875.
[77] C.-P. Huang, Y.-H. Huang, Appl. Catal. A Gen. 346 (2008) 140–148.
[78] P. Verma, V. Shah, P. Baldrian, P. Stopka, Chemosphere 54 (2004) 291–295.
[79] N.N. Fathima, R. Aravindhan, J.R. Rao, B.U. Nair, Chemosphere 70 (2008) 1146–1151.
[80] N. Inchaurrondo, J. Cechini, J. Font, P. Haure, Appl. Catal. B Environ. 111–112 (2012) 641–648.
[81] Y. Zhan, H. Li, Y. Chen, J. Hazard. Mater. 180 (2010) 481–485.
[82] J.J. Pignatello, E. Oliveros, A. MacKay, Crit. Rev. Env. Sci. Technol. 36 (1) (2006) 1–84.
[83] F. Emami, A.R. Tehrani- Bagha, K. Gharanjig, F.M. Menger, Desalination 257 (2010) 124–128.